ELSEVIER

Catalysis Today 70 (2001) 91–105

CATALYSIS TODAY

www.elsevier.com/locate/cattod

Interaction of N_2, CO and NO with Cu-exchanged ETS-10: a compared FTIR study with other Cu-zeolites and with dispersed Cu_2O☆

S. Bordiga[a,*], C. Pazé[a], G. Berlier[a], D. Scarano[a], G. Spoto[a], A. Zecchina[a], C. Lamberti[b]

[a] *Dipartimento di Chimica IFM, I-10125 Via P. Giuria 7, Torino, Italy*
[b] *Dipartimento di Chimica IFM, Unità INFM Torino-Università, I-10125 Via P. Giuria 7, Torino, Italy*

Abstract

After a brief overview of the reasons why, in spite of the high fraction of framework Ti(IV) atoms, Engelhard titanosilicate (ETS-10) cannot be used as competitive catalyst in partial oxidation reactions, we draw the attention on the fact that the high cation density of ETS-10 can be the key property for potential new catalytic applications of this recent material. Among all, cation exchange with Cu^{2+} can yield to Cu-ETS-10, a promising material for environmental catalysis. We so present a detailed characterization of this material using N_2, CO and NO as probe molecules. In spite of the rather high complexity of the obtained spectra, a comparison with similar experiments (described in the literature or ad hoc performed for this work) on other Cu-exchanged zeolites and on Cu_2O dispersed on silica and on MCM-41, allows a full interpretation of the spectroscopic properties. It is shown that copper is present both as counterion and in the form of Cu_2O nanoclusters dispersed in the ETS-10 channels and in the external surface. Finally, IR spectroscopy has been used to demonstrate that Cu-ETS-10 is active in the decomposition of NO. © 2001 Published by Elsevier Science B.V.

Keywords: Titanosilicate; ETS-10; FTIR spectroscopy; CO; N_2; NO; Cu-exchanged zeolites; NO decomposition

1. Introduction

Engelhard titanosilicate (ETS-10) is a new microporous crystalline material belonging to the family of Ti-substituted silicates containing Ti in octahedral coordination [1,2]. Because of its inherently disordered nature, preventing the use of conventional diffraction approaches, the structure of ETS-10 was solved only 5 years after its synthesis by Anderson et al. [3–5]. To achieve this goal, high resolution transmission electron microscopy, powder X-ray diffraction, solid state NMR and molecular modeling techniques were used. They proved that ETS-10 framework is composed of corner-sharing SiO_4 tetrahedra and TiO_6 octahedra linked through bridging oxygen atoms, and that two sets of perpendicular 12-ring channels having an elliptical cross-section 7.6 Å × 4.9 Å are present. The recent single crystal study by Wang and Jacobson [6] has confirmed the model of Anderson et al. To have a complete view on the recent progresses obtained in the synthesis and in the characterization of microporous titanosilicates and mixed octahedra–tetrahedra framework oxides, the reader should refer to the review of Rocha and Anderson [7].

☆ Paper submitted for publication on Catalysis Today as an article in the special issue devoted to Jean-Claude Lavalley's 60th birthday entitled: "IR Spectroscopy Applied to Catalysis".

* Corresponding author. Tel.: +39-011-6707858; fax: +39-011-6707855.
E-mail address: bordiga@ch.unito.it (S. Bordiga).

0920-5861/01/$ – see front matter © 2001 Published by Elsevier Science B.V.
PII: S0920-5861(01)00410-2

It is worth noticing that the TiO_6 octahedra in ETS-10 are linked together with formation of linear ···–O–Ti–O–Ti–O–Ti–O–··· chains (each Ti atom being also linked, in the perpendicular plane, to four Si atoms through oxygen bridges). Sankar et al. [8], performing Ti K-edge extended X-ray absorption fine structure (EXAFS), have confirmed the octahedral coordination of Ti proposed in Refs. [3–5] highlighting the local structure around titanium. The presence of such linear ···–O–Ti–O–Ti–O–Ti–O–··· chains represents the realization of a monoatomic quantum wire hosted in a silicaceous matrix exhibiting interesting and promising optical properties [9–11].

The octahedral coordination of Ti in ETS-10 is different from that found in other titanosilicates such as Ti-β [12] or TS-1 [13–15], where Ti is tetrahedrally coordinated, like silicon, to four framework O atoms. This implies that Ti atoms in ETS-10 have already saturated their coordination sphere and that they cannot interact with molecules adsorbed in the channels. This was demonstrated by Sankar et al. [8], who have showed that the Ti K-edge XANES spectra of ETS-10 are not affected by interaction with ligands, contrarily to what observed for TS-1, where Ti is able to modify reversibly its coordination sphere [14–16]. As a consequence, ETS-10 is not suitable for oxidation catalysis employing H_2O_2 under mild conditions as is the case of TS-1 [13,14].

It should therefore be concluded that the octahedral coordination of titanium in ETS-10 makes the chemistry of Ti of no catalytic interest. Nevertheless, the insertion of a Ti(IV) atom in a 6-fold coordinated framework site implies the transfer of two electrons to the lattice which so becomes negatively charged. The resulting negative charge of the framework $Si_{40}Ti_8O_{104}{}^{16-}$ unit is balanced by the presence of Na^+ and K^+ counterions located in the channels [17–19]. The high number of framework Ti (Si/Ti = 5) and the fact that each Ti needs the presence of two monovalent counterions, make the number of counterions rather high. This fact implies that ETS-10 is a microporous material exhibiting remarkable cation exchange capabilities. As a consequence, ETS-10 shows potential application in the fields of bi-functionality induced by metal loading [7], of photocatalysis [7,20] and of base catalysis [7] (vide infra).

It has been shown that alkali-metal cations can easily substitute the original Na^+ and K^+ counterions leading to the Li^+, Na^+, K^+, Rb^+ or Cs^+ forms [10,21] and that the cation exchange with alkali-metal cations represent a reliable mean to tune the basicity of the material. This property has been exploited by Anderson and co-workers [22] and by the group of Sivasanker [23,24], who have studied the bifunctional reforming reaction of hexane to benzene over Pt-supported basic ETS-10. The high basicity of ETS-10 is evidenced in the conversion of isopropanol to acetone [25] and in the dehydration of *t*-butanol [7].

The high cation density suggests that the exchange capacity towards di-valent cations should be facilitated. Indeed, ETS-10 has been shown to be particularly selective in the hosting of Pb^{2+} [26] and Cd^{2+} [7] cations. Very recently, Otero Areán et al. [27] reported an IR investigation on Mg^{2+}-ETS-10. Finally, the group of Ragaini [28–31] has performed an extensive study of the Fisher–Tropsch chemistry performed with cobalt and ruthenium-exchanged ETS-10.

The promising exchange capabilities of this titanosilicate, together with the fact that copper-exchanged zeolites have recently attracted a great interest as catalyst for the direct conversion of NO into N_2 and O_2 [32–35] have encouraged us to prepare a Cu^{2+}-ETS-10 sample. In this contribution, we will describe for the first time the spectroscopic properties of N_2, CO and NO interacting at liquid nitrogen temperature with copper cations hosted inside ETS-10. Comparison will be made with IR data obtained on Cu-ZSM-5 [36], Cu-Y [37], Cu-mordenite [38], Cu-β [39] and on Cu grafted on MCM-41 [40]. Comparison will also be made with the IR spectra of N_2, CO and NO adsorbed on other cationic form of ETS-10. To understand the spectroscopy of CO on Cu-ETS-10, a comparison with the spectra of carbon monoxide dosed on Cu_2O dispersed on silica [41] and on MCM-41 [40] will be made. In this contribution, new IR experiments have been ad hoc performed by dosing N_2 and NO on Cu_2O dispersed on silica.

2. Experimental

The ETS-10 sample used in this study was kindly supplied by Engelhard (Iselin, NJ). Chemical anal-

ysis showed a Na^+/K^+ ratio of 2.64, and powder X-ray diffraction showed good crystallinity and confirmed the expected structure type. No additional diffraction lines were found. After conventional ion exchange procedures with $NaNO_3$, as described elsewhere [21], the achieved Na^+/K^+ ratio was 5.30. We shall refer in the following to this sample as the sodium-exchanged form or as Na-ETS-10. MCM-41 sample, with $Si/Al \approx 20$ and pore diameter of ≈40 Å, has been kindly supplied by EniTecnologie laboratories of San Donato Milanese (MI), Italy. Commercial silica (Aerosil from Degussa, s.a. $\approx 330\,m^2\,g^{-1}$) has been used.

To obtain a Cu-exchanged ETS-10, Na-ETS-10 powder was exchanged twice with $Cu(NO_3)_2$ (Aldrich, analytical grade) as described in Ref. [42] for the preparation of Cu^{2+}-ZSM-5. The so-obtained samples will be hereafter labeled as Na-Cu-ETS-10(A), and Na-Cu-ETS-10(B), after the first and second exchange, respectively. MCM-41- and silica-supported Cu_2O samples have been prepared by impregnation of the support with an aqueous solution of $Cu(NO_3)_2$ and followed by a high-temperature treatment in vacuo (873 K for MCM-41 and 1073 K for silica) as extensively described in Refs. [40,41], respectively. The latter sample is labeled as Cu_2O/SiO_2 (10% Cu/Si wt. ratio), while the former is labeled as Cu-MCM-41 and Cu_2O/MCM-41 for low (1% Cu/Si wt. ratio) and high (10% Cu/Si wt. ratio) Cu loading, respectively.

Samples for IR studies were compressed into self-supporting wafers and degassed in dynamic vacuum (residual pressure $<10^{-4}$ Torr) inside an IR cell allowing in situ high-temperature treatments, gas dosage, and low-temperature measurements to be made. Na-ETS-10, Na-Cu-ETS-10(A) and Na-Cu-ETS-10(B) were degassed at 673 K for 2 h, while Cu-MCM-41, Cu_2O/MCM-41 and Cu_2O/SiO_2 samples were degassed at 873 K (MCM-41) and 1073 K (silica). The IR spectra were recorded, at $2\,cm^{-1}$ resolution, on a Bruker IFS66 FTIR spectrometer. Although the IR cell was permanently cooled with liquid nitrogen, the actual sample temperature (under the IR beam) was likely to be ca. 100–110 K. The wafer spectrum taken before gas dosage was used as a blank. All spectra shown in this paper are blank subtracted. UV–Vis diffuse reflectance experiments have been performed with a Varian CARY5 spectrophotometer.

3. Results and discussion

Copper zeolites can be prepared in over-exchanged form [32] by exchange with water solution of cupric salts. For over-exchanged form we intend a form, containing more than one Cu^{II} ion per two framework Al. These over-exchanged ($Cu/Al > 0.5$) zeolites show the highest activity for the decomposition of nitrogen oxides.

With the aim of reaching high exchange levels, since 1992, our group has proposed an alternative exchange procedure consisting in the interaction of CuCl in the vapor phase with the zeolites in the protonic form [32,43–46], resulting in the $Si(OH^+)Al + CuCl_{gas} \rightarrow Si(OCu^+)Al + HCl_{gas}$ reaction. This exchange approach allows the direct insertion of cuprous ions and the virtual achievement of a 200% exchange (i.e. a Cu/Al ratio of 1). We were unable to follow the same route for the preparation of a Cu-ETS-10 sample, since it needs thermal treatments at a temperature where the protonic form of ETS-10 is unstable. For this reason, the conventional exchange route has been adopted (see Section 2). Due to the potentially high cation exchange capabilities of ETS-10 discussed in Section 1, this inconvenience is of secondary importance for the achievement of rather high copper loadings.

It must be, however, underlined that, over Cu-exchanged zeolites catalysts prepared by ion exchange with aqueous solutions of a Cu^{2+} salt, IR, UV–Vis, EPR, XPS, XANES and EXAFS studies have shown [32,42,47,48] good evidence for the presence of both isolated Cu^{2+} and Cu^+ ions and of several oxocations such as $[Cu–O–Cu]^+$ and $[Cu–O–Cu]^{2+}$, together with copper oxide aggregates, Cu_2O nano-crystals. In view of the high Cu loading, a great heterogeneity of copper species is expected for Na-Cu-ETS-10 samples.

It is widely recognized [42,48–51] that an effective reduction of samples containing hydrated cupric ions can be obtained during activation under dynamic *vacuum*. This fact is often called "self-reduction" of Cu^{2+}. Different chemical $Cu^{2+} \rightarrow Cu^+$ pathways have been proposed in the literature to explain the process. We will not enter in this complex debate here and we shall just accept the phenomenon as a matter of fact. For a more detailed discussion, the reader should refer to the recent works of Dossi et al. [51] and Turnes Palomino et al. [42]. On these bases, we expect that also in our

case Cu^+ will be certainly present after activation in vacuo at high temperature.

3.1. UV–Vis study of the prepared an activated samples

Na-ETS-10 sample has no absorption in the 30,000–7500 cm^{-1} range and exhibits a sharp edge at ≈32,600 cm^{-1} (≈4.03 eV) due to the $Ti^{4+}O^{2-} \rightarrow Ti^{3+}O^-$ ligand to metal charge transfer (LMCT) [9–11] (see spectrum 1 in Fig. 1). Since the energy value of this LMCT is dictated by quantum confinement effects in the mono-atomic ···–O–Ti–O–Ti–O–··· quantum wire, we do not expect any significant shift upon cation exchange with $Cu(NO_3)_2$. The invariance of the LMCT edge for Na-Cu-ETS-10(B) sample (i.e. the sample exchanged twice) is demonstrated in Fig. 1 (spectrum 2). In this spectrum, the appearance of a new band centered around 12,700 cm^{-1} (typical d–d transition of the d^9 Cu^{2+} cation) is the direct proof that cupric cations have been successfully inserted in the ETS-10 sample. Dehydration of the sample by evacuation at 383 K causes an increase of the d–d transition intensity together with a blue shift of the maximum at 13,400 cm^{-1} (spectrum 3 in Fig. 1). This is exactly the expected behavior of the d–d band upon loss of the coordinated water molecules, and similar spectra have recently been reported for a Cu^{2+}-ZSM-5 sample [42]. The same experiments performed on the Na-Cu-ETS-10(A) sample (not reported for brevity) yield to similar although less intense spectra, as expected for a less-exchanged sample.

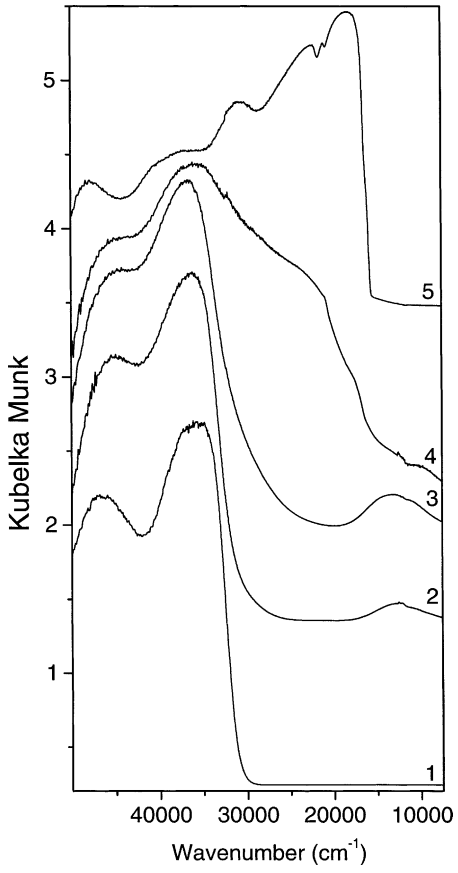

Fig. 1. UV–Vis spectra collected in the reflectance mode of: (1) hydrated Na-ETS-10; (2) hydrated Na-Cu-ETS-10(B); (3) Na-Cu-ETS-10(B) dehydrated at 383 K; (4) Na-Cu- ETS-10(B) dehydrated at 673 K; (5) Cu_2O bulk. The UV–Vis spectrum of the Cu_2O/SiO_2 sample is not reported, since its edge corresponds to that of Cu_2O bulk [41].

Upon increasing the thermal treatment temperature (spectrum 4 in Fig. 1), the spectrum of sample (B) (and sample (A) as well, not reported) change abruptly. However, the modification is completely different from that observed for Cu^{2+}-ZSM-5 [42]. Starting from 473 K, in Cu^{2+}-ZSM-5 a progressive decrement of the d–d band is observed up to its total disappearance on samples activated at 673 K, witnessing that $Cu^{2+} \rightarrow Cu^+$ reduction is occurring [42]. On sample Na-Cu-ETS-10(B), the appearance of two strong and complex edges in the 16,500–20,000 cm^{-1} region is observed. To understand this phenomenon, a comparison with the UV–Vis spectrum of Cu_2O is useful (spectrum 5 in Fig. 1). In fact, cuprous oxide has a well-defined gap at 16,280 cm^{-1} (evidenced by the very sharp edge in Fig. 1) which coincides with the first edge of Cu-ETS-10(B) at 16,300 cm^{-1}. This can be explained in terms of the formation of a consistent amount of Cu_2O particles. The second edge at about 20,000 cm^{-1} is slightly blue-shifted: we think that this is due to confinement effects in Cu_2O nano-particles (these effects can be observed only if the size of the cuprous oxide crystals is in the nanometer/subnanometer scale, see the abundant literature quoted in Ref. [10]). In conclusion, the UV–Vis spectra reveal a bimodal distribution of Cu_2O particles. We think that the larger ones are located on the external surface, while the smaller ones are encaged inside the zeolite framework. Due to their smaller

dimension, the particles encaged in the zeolite will play a dominant role in the adsorptive properties.

Upon thermal treatment at high temperature, the d–d band of the Cu^{2+} is still observable (see inflection at about 12,000 cm^{-1}). However, the dominating features of Cu_2O in the region of interest prevent a quantification. Based on our experience, we shall assume that most of the cupric cations have been reduced to Cu^+ and that they belong to two families: extraframework Cu^+ counterions (like in Cu^+-ZSM-5) and Cu^+ ions in Cu_2O particles. This assumption will be strongly confirmed by the IR studies reported hereafter.

The presence of Cu_2O in Cu-zeolites prepared with this cation exchange method is not unexpected, and already claimed by several groups (see above). Note also that we have already used the same preparation method for supporting Cu_2O on silica or on MCM-41 [40,41]. It is in fact well known that CuO, formed by thermolysis of $Cu(NO_3)_2$, has the propensity to lose oxygen atoms when heated at high temperatures in vacuo: this implies that a thermal treatment of the samples causes the "self-reduction" of CuO into Cu_2O. We think that the formation of Cu_2O particles in ETS-10 is likely favored by the high copper concentration inside the exchanged (hydrated) material.

3.2. IR spectroscopy of adsorbed N_2

The use of di-nitrogen as probe molecule is particularly suitable, since the N–N stretching frequency is expected to appear in two definitively different spectral regions for the $Na^+\cdots N_2$ and for the $Cu^+\cdots N_2$ adducts. It is a matter of fact that the interaction of N_2 with alkali-metal cations, being only of electrostatic nature, yields a $\bar{\nu}$(NN) in the 2335–2325 cm^{-1} range [21,52,53], while the interaction with cuprous ions inside zeolites gives a $\bar{\nu}$(NN) in the 2300–2295 cm^{-1} region [36,54]. For sake of comparison, Table 1 reports the N–N stretching frequencies of di-nitrogen adducts in zeolites, zeotypes and on Cu_2O dispersed on silica. The use of N_2 will thus allow a spectroscopic determination of the exchange level for accessible cations, i.e. those present in the 12-membered rings forming the channels.

Fig. 2 reports the IR spectra of di-nitrogen dosed at increasing equilibrium pressures on Na-ETS-10, Na-Cu-ETS-10(A) and Na-Cu-ETS-10(B), parts (a), (b) and (c), respectively. Part (a) reports the already known sharp and well-defined $\bar{\nu}$(NN) band of $Na^+\cdots N_2$ adducts in ETS-10, at 2333 cm^{-1} [21]. The spectra reported in part (b) show the same band, now reduced at about 50%, and a new broader absorption in the 2300–2275 cm^{-1} range. The fact that the former component is further reduced, while the latter is further increased after a second cation exchange (part c), allows the straightforward assignment of the low frequency band to $Cu^+\cdots N_2$ adducts. By measuring the intensity decrement of the 2333 cm^{-1} band, it is inferred that about 50 and 70% of the original Na^+ accessible cations have been substituted after the first and the second copper exchange. Nothing can be said for inaccessible cations.

Table 1
N–N stretching frequencies of di-nitrogen adducts in zeolites, zeotypes, and on supported Cu_2O

Sample	$\bar{\nu}$(NN) (cm^{-1})	Reference
Na-ETS-10	2333	This work and [21]
K-ETS-10	2331.5	[21]
Na-Cu-ETS-10(A) Na site	2331	This work
Na-Cu-ETS-10(A) Cu^+ site	2281	This work
Na-Cu-ETS-10(B) Na site	2329	This work
Na-Cu-ETS-10(B) Cu^+ site	2285	This work
Cu_2O/SiO_2	2283	This work
Cu^+-mordenite	2299	[54]
Cu^+-ZSM-5	2295	[36]

It is worth noticing that the 2285 cm^{-1} band is more resistant to degassing than that at 2333 cm^{-1}. This reflects the higher interaction energy of the $Cu^+\cdots N_2$ adduct with respect to the $Na^+\cdots N_2$ one.

The band ascribed to $Cu^+\cdots N_2$ adducts is rather broad (FWHM = 17 cm^{-1}), especially when compared with that of the 2333 cm^{-1} band (FWHM = 2.5 cm^{-1}), or with the width of the band observed for $Cu^+\cdots N_2$ adducts in a Cu^+-ZSM-5 prepared from CuCl (FWHM = 6 cm^{-1} [36]). This observation proves that the Cu^+ cations in an ETS-10 sample obtained after thermal activation of the corresponding cupric sample have heterogeneous structures. The value of the frequency maximum merits few comments. In fact, in sample (B), it is located at 2285 cm^{-1} (at $P(N_2)$ = 5 Torr): this frequency is definitively lower than those obtained by Kuroda et al.

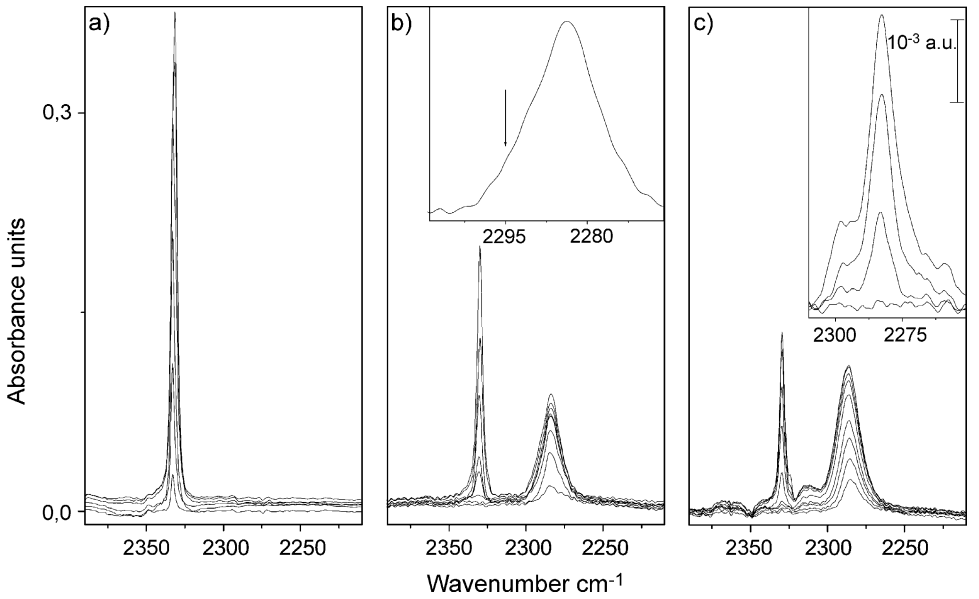

Fig. 2. Liquid nitrogen IR spectra of N_2 dosed at increasing equilibrium pressures (from 10^{-2} to 5 Torr; 1 Torr ≈ 133.3 Pa) on Na-ETS-10, Na-Cu-ETS-10(A) and Na-Cu-ETS-10(B) samples, parts (a), (b) and (c), respectively. The inset in part (c) reports the same experiment performed on the Cu_2O/SiO_2 sample. The inset in part (b) reports a magnification of the highest coverage spectrum in the 2310–2265 cm^{-1} range; the vertical arrow indicates the high frequency shoulder attributed to the N–N stretching frequency of N_2 adsorbed on isolated Cu^+ counterions inside the ETS-10 channels.

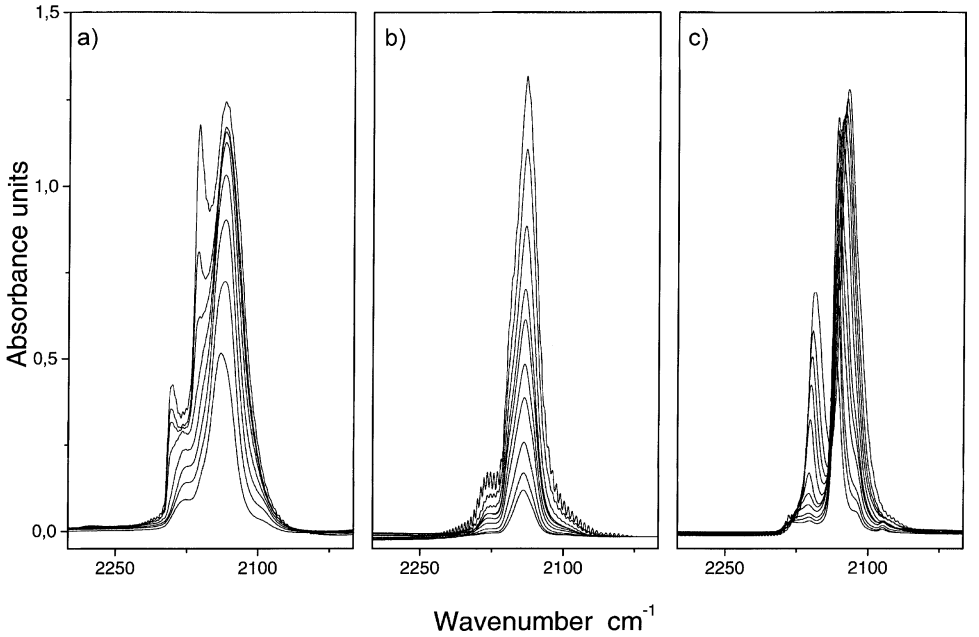

Fig. 3. (a) IR spectra of CO dosed on Na-Cu-ETS-10(B) sample at about 77 K; (b) IR spectra of CO dosed on Na-Cu-ETS-10(B) sample at RT; (c) IR spectra of CO dosed on Cu_2O/SiO_2 (pressures between 10^{-2} and 10 Torr).

[54] on Cu^+-mordenite (2299 cm^{-1}) or by Bordiga and co-workers [36] on Cu^+-ZSM-5 (2295 cm^{-1}).

To advance a reasonable explanation of this observation, we have performed the same experiment on the Cu_2O/SiO_2 sample (see Fig. 3c). N_2 dosed on Cu_2O/SiO_2 gives rise to a very weak absorption at 2283 cm^{-1} (FWHM = 10 cm^{-1}), together with a high frequency shoulder developing only at the high N_2 pressures. On the basis of a previous SEM and TEM study on pure and silica-supported Cu_2O [41], we ascribe the 2283 cm^{-1} band to $Cu^+\cdots N_2$ adducts formed on Cu^+ sites of the unpolar $Cu_2O(1\,1\,1)$ facelet or terrace. The high frequency band is tentatively ascribed to $Cu^+\cdots N_2$ adducts formed, either on less dominant facelets, or on the less coordinatively unsaturated cuprous cation of the (1 1 1) face [41].

From these considerations, we conclude that the broad absorption in the 2300–2275 cm^{-1} range, on (A) and (B) samples is due to the simultaneous presence of a dominant band at 2285 cm^{-1} (due to N_2 adsorbed on Cu_2O nano-crystals) and to a less intense component at about 2295 cm^{-1} (due to N_2 adsorbed on Cu^+ counterions). The latter component can be better appreciated in the inset of Fig. 2b, where a magnification of the highest coverage spectrum is reported in the 2310–2265 cm^{-1} range.

By comparing the intensity of the band due to $Cu^+\cdots N_2$ adducts on Cu_2O/SiO_2 and that measured on Na-Cu-ETS-10(B), we infer that Cu_2O is under highly dispersed form. This observation agrees with the observed energy gap of the Cu_2O particles hosted in ETS-10 (20,000 cm^{-1}), blue-shifted with respect to that of bulk Cu_2O, due to confinement effects (see Fig. 1).

The minor IR absorption at 2315 cm^{-1} observed at the highest pressures in Fig. 2c is of difficult attribution. We just mention that it has not been detected in the sample Na-Cu-ETS-10(A).

3.3. IR spectroscopy of adsorbed CO

The IR spectra (recorded at nominal 77 K temperature and at RT) of increasing doses of CO on the Na-Cu-ETS-10(B) sample are reported in Fig. 3a and b, respectively. As CO does not interact with Na^+ cations at RT, the spectra reported in Fig. 3b concern only copper carbonyl adducts. As far as low-temperature spectra are concerned, the band of the $Na^+\cdots CO$ adducts formed on the fraction of unexchanged sodium cations cannot be observed as well, since it is totally overshadowed by the much strong spectral features of Cu^+ carbonyls (which appear in the same spectroscopic region, but have a considerably higher extinction coefficient due to the relevant role played by π-back donation in the $Cu^+\cdots CO$ bond [46]).

The spectroscopy of CO interacting with cuprous ions in ETS-10 is rather complex: the spectra recorded at RT and the low coverage spectra of the low-temperature experiment show the presence of two very broad bands (in the 2160–2120 cm^{-1} and in the 2200–2170 cm^{-1} intervals). The broad nature of these bands well agrees with the heterogeneity of Cu^+ cations already monitored by N_2 (vide supra, Fig. 2). At the highest P_{CO}, the low-temperature spectra (in Fig. 3a) show two new, and rather narrow, bands at 2191 and 2162 cm^{-1}. This fact contrasts with the broad character of the precursors described before. In spite of the evident complexity of the spectra reported in Fig. 3 (a and b), their interpretation can be made in a straightforward manner on the basis of a detailed comparison with the results obtained on Cu_2O/SiO_2 and on Cu^+-ZSM-5, Cu^+-β, Cu^+-mordenite and Cu^+-Y (Figs. 3c and 4, respectively).

Of special utility is the comparison with the spectra of CO on Cu_2O/SiO_2 (Fig. 3c). According to Ref. [41], the band at 2132 cm^{-1} (lowest dosage) progressively shifting to 2127 cm^{-1} upon increasing the CO pressure, is assigned to $Cu^+\cdots CO$ adducts formed on mono-coordinated Cu^+ sites of the unpolar $Cu_2O(1\,1\,1)$ facelets of Cu_2O microcrystals and the bathochromic shift is ascribed to the progressive building up of lateral interactions among adjacent adsorbates. Upon increasing the P_{CO}, two components at 2162 and 2127 cm^{-1} show up, which are assigned to the asymmetric and symmetric stretching modes of the complex $Cu^+\cdots(CO)_2$ [41]. Both bands undergo a red shift (from 2162 to 2154 and 2127 to 2120 cm^{-1}, respectively, Table 2) with CO coverage. Also in this case, the shift is ascribed to lateral interactions among adsorbates. The spectra of CO on pure Cu_2O polycrystals are similar and the frequencies of the relevant bands are reported in Table 2. In no cases, the formation of $Cu^+\cdots(CO)_3$ adducts has been observed on Cu_2O.

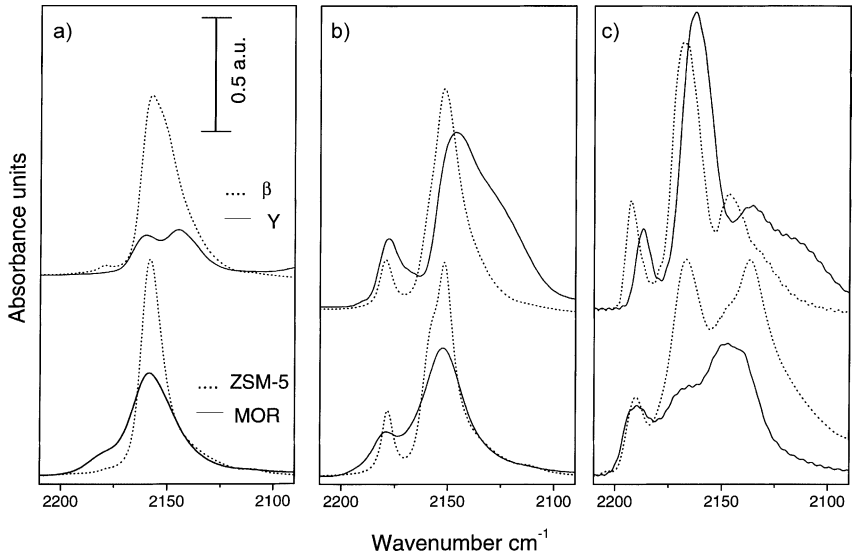

Fig. 4. IR spectra of CO dosed, at liquid nitrogen temperature, on Cu^+-ZSM-5 (bottom dotted lines), Cu^+-mordenite (bottom full lines), Cu^+-β (top dotted lines), and Cu^+-Y (top full lines) zeolites. Parts (a), (b) and (c) reports low, medium and high CO equilibrium pressure spectra, respectively, approximately corresponding to mono-, di- and tri-carbonyl complexes.

Coming now to the spectra of CO on Cu^+-zeolites (ZSM-5, β and mordenite), it is worth recalling that at low CO equilibrium pressures (Fig. 4a), a single band is observed for the monocarbonylic complex (see $\bar{\nu}$(CO) in Table 2). Contrarily to what observed for both Cu_2O/SiO_2 and pure Cu_2O, the position of these bands is not affected by the CO equilibrium pressure, since adsorbate–adsorbate interactions are not present.

Table 2
C–O, $\bar{\nu}_a(CO)_m$ ($m = 1, 2, 3$), stretching frequencies of carbonyl adducts in Cu^+-zeolites, Cu_2O/silica and Cu_2O[a]

Sample	$\bar{\nu}$(CO) (cm^{-1})	$\bar{\nu}_l(CO)_2$ (cm^{-1})	$\bar{\nu}_h(CO)_2$ (cm^{-1})	$\bar{\nu}_l(CO)_3$ (cm^{-1})	$\bar{\nu}_m(CO)_3$ (cm^{-1})	$\bar{\nu}_h(CO)_3$ (cm^{-1})	Reference
Cu^+-ZSM-5	2157	2151	2178	≅2138	2167	2192	[36]
Cu^+-β	2157	2152	2180	2146	2167	2193	[39]
Cu^+-mordenite	2159	2150	2180	≅2145	≅2165	2190	[38]
Cu^+-Y Site II	2159	2148	2178	≅2138	2165	2188	[37]
Cu^+-Y Site II*	2143	2135	2168	≅2138	2165	2188	[37]
Cu^+-MCM-41	2159	2152	2180	2138	2171	2194	[40]
Na-Cu-ETS-10(B) isolated Cu^+ site	≅2155	≅2150	≅2180	≅2135	2162	2191	This work
Na-Cu-ETS-10(B) Cu_2O site	2141	≅2130	≅2165	Not observed	Not observed	Not observed	This work
Cu_2O/SiO_2	2132–2127	2127–2120	2162–2154	Not observed	Not observed	Not observed	[41] and this work
Bulk Cu_2O	2127–2121	2121–2113	2158–2145	Not observed	Not observed	Not observed	[41]
Cu_2O/MCM-41	≅2141	≅2133	≅2155	Not observed	Not observed	Not observed	[40]
Na-ETS-10	2178	Not observed	Not observed	Not observed	Not observed	Not observed	[21]

[a] When needed, label "a" (a: l, m, h) refers to low, medium and high frequency components of the adduct. For comparison, also the $\bar{\nu}$(CO) observed on Na-ETS-10 is reported. For Cu_2O/SiO_2 and bulk Cu_2O samples, an interval of frequencies has been reported for $\bar{\nu}$(CO), $\bar{\nu}_l(CO)_2$ and $\bar{\nu}_h(CO)_2$, since the frequency position of the band was pressure dependent [41]. Very recently, the assignment of the band here labeled as $\nu_l(CO)_3$ to a third, low frequency component of the $Cu^+(CO)_3$ complex inside zeolites has been questioned, and the alternative hypothesis that it could be due to liquid-like CO physisorbed on the zeolitic walls has been put forward [55].

On Y zeolite, the situation is slightly more complex since two different $Cu^+\cdots CO$ adducts characterized by $\bar{\nu}(CO) = 2159$ and $2143\,cm^{-1}$ are observed. This IR evidence is supported by Rietveld refinement of XRPD data collected at the BM16 beamline at the ESRF, where two different cationic sites have been determined in the supercage [37]. These sites have been labeled as II and II*: the second lies in a more shielded position and is responsible of the band at $2143\,cm^{-1}$. On all zeolites, by increasing the CO equilibrium pressure (Fig. 4b), the formation of $Cu^+\cdots(CO)_2$ adducts is observed, as proved by the formation of two new bands at 2135–2151 and 2168–2178 cm^{-1} (Table 2) assigned to the asymmetric and symmetric stretching modes of the complex [36,38,39]. According to the presence of two different sites (II and II*) in Y zeolite, two doublets have been observed.

A further increase of the equilibrium pressure (Fig. 4a), causes a total (ZSM-5 [43], β [39]) or a nearly total (Y [37]) $Cu^+\cdots(CO)_2 \rightarrow Cu^+\cdots(CO)_3$ transformation, accompanied by the appearance of a new triplet of IR active bands at 2138–2146, 2165–2167, and 2188–2193 cm^{-1} (Table 2). This triplet has been interpreted as the IR manifestation of $Cu^+\cdots(CO)_3$ complexes with a symmetry rather lower than C_{3v} [36,38,39,43] (only two IR active band are in fact expected in the case of a C_{3v} symmetry). It is, however, worth recalling that the assignment of the band at lower frequencies to the third, low frequency, component of the $Cu^+(CO)_3$ complex has been recently questioned [55]. It is a matter of fact that the low frequency band lies in the 2135–2146 cm^{-1} interval, i.e. very close to the absorption of physically adsorbed CO ($2138\,cm^{-1}$) [56]. We shall not enter in this debate here, since the problem of the local symmetry of $Cu^+(CO)_3$ complexes hosted in zeolites is not relevant for the present work. As far as Cu-mordenite is concerned, the additional presence of cations in the less accessible side pocket sites leads to the simultaneous presence of mono-, di- and tri-carbonyl adducts even at the higher equilibrium pressures [38], a fact which is originating a broader and rather unresolved IR spectrum (Fig. 4c). An interesting property of the $Cu^+\cdots(CO)_3$ adducts is represented by the small half-width of the IR bands, which is not influenced by the heterogeneity character of the sites. This relevant fact is explained in terms of the high complexing power of the CO molecules, which are able to extract the Cu^+ cations from the original positions. In other words, the $Cu^+(CO)_3$ complexes do not have "memory" of the structure of the original Cu^+ sites. This last statement has been supported by independent EXAFS [46,55] and synchrotron radiation XRPD [37] experiments.

Coming to Cu_2O supported on MCM-41 [40], we just underline that samples with low copper content (like sample Cu-MCM-41, Cu/Si = 1 wt.%) show CO bands very similar to those observed in zeolites, while samples with high Cu content (sample Cu_2O/MCM-41, Cu/Si = 10 wt.%) show additional components similar to those of CO on Cu_2O (see Table 2). These observations led to the conclusion that the impregnation with copper nitrate is a good method for grafting isolated Cu^+ cations in the MCM-41 inner surface when low copper loading are used, and that the method gives preferentially Cu_2O microparticles at high Cu loading [40].

After this essential comparison with already understood systems, we can discuss the IR spectra of CO dosed on Na-Cu-ETS-10(B) sample. The broad component with a distinct maximum at $2141\,cm^{-1}$ appearing at the lowest dosage can be ascribed to $Cu^+\cdots(CO)$ complexes formed on Cu_2O nano-crystals. On the basis of the data concerning Cu^+ on zeolites, the shoulder around $2155\,cm^{-1}$ is assigned to CO adsorbed on atomically dispersed cuprous counterions in ETS-10. Upon increasing P_{CO}, both species are transformed into $Cu^+\cdots(CO)_2$ complexes. The two $\bar{\nu}(CO)_2$ frequencies of $Cu^+(CO)_2$ complexes (see Table 2) do not shift with coverage: this is the proof that the size of the Cu_2O nano-crystals on ETS-10 is so small that the lateral interactions among adsorbed CO molecules in ordered bi-dimensional layers cannot build up.

The narrow bands at 2191 and $2162\,cm^{-1}$ (high P_{CO}) occur at frequencies very close to those reported for $Cu^+\cdots(CO)_3$ adducts hosted in Cu^+-zeolites (see Table 2): they are consequently assigned to tri-carbonyl complexes formed on Cu^+ counterions inside ETS-10. The narrow character of the $Cu^+(CO)_3$ bands is also typical of tricarbonylic complexes.

The spectroscopy of CO dosed on Na-Cu-ETS-10(A) sample (not reported for brevity) is similar to that reported in Fig. 3a and b, the only difference consisting in the relative intensity of the bands ascribed to CO adsorbed on Cu_2O microcrystals.

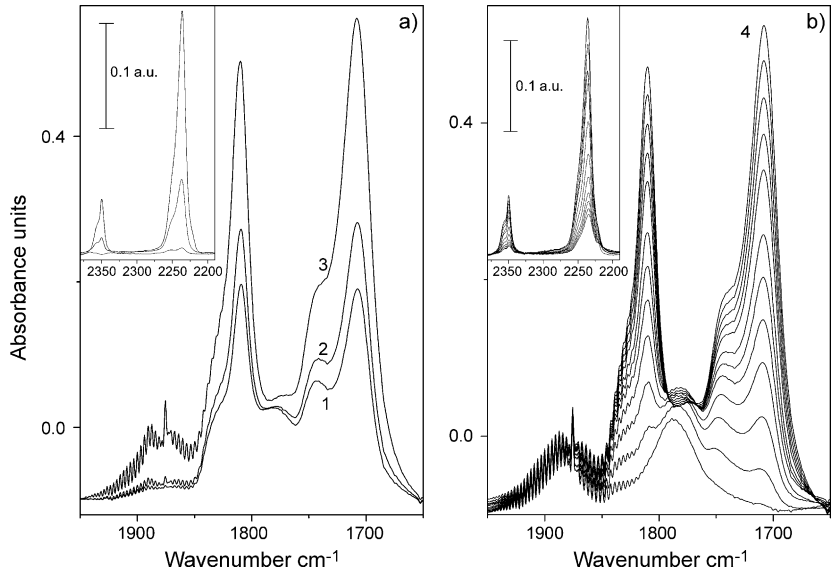

Fig. 5. IR spectra of NO dosed on Na-Cu-ETS-10(B) sample as a function of the temperature increase from liquid nitrogen temperature to RT. (a) First stage; (b) final stages. During stage (a), the P_{NO} increases from about 10^{-1} (at $T < 150$ K, line 1) to 10 Torr (at $T \cong 150$ K, line 3). During stage (b), the pressure is constant (about 10 Torr), and the temperature is between 150 (line 4) and 273 K (line 15). The insets report the 2380–2190 cm^{-1} region, where some products of the NO decomposition reaction are expected.

3.4. IR spectroscopy of adsorbed NO

Like N_2 and CO at 77 K, NO is a probe of cationic sites in Cu-exchanged zeolites. However, unlike the N_2 and CO probes, when the temperature increases up to RT, NO can yield a complex redox chemistry related to nitric oxide decomposition. This is shown in the experiment reported in Fig. 5, where the spectra of NO initially dosed at low temperature on sample Na-Cu-ETS-10(B), and the spectra obtained during the successive gradual warming to RT are reported. During the warming procedure, the P_{NO} changes abruptly from 7×10^{-2} to 10 Torr (at about 150 K).

The bottom curve of Fig. 5a is the IR spectrum (curve 1) of adsorbed NO at the nominal liquid nitrogen temperature ($P_{NO} = 7 \times 10^{-2}$ Torr NO). This spectrum is rather complex, showing two dominant peaks at 1708 and 1809 cm^{-1} and two less intense peaks at 1743 and 1775 cm^{-1} and a shoulder around 1885 cm^{-1}. The absence of any significant band in the 1915–1880 cm^{-1} range, where the N–O stretching frequency of $Cu^{2+}\cdots(NO)$ adducts is expected [32,36,57], implies that nearly all cupric ions in accessible positions have been reduced to cuprous ions during the thermal activation and that the observed band must be ascribed to $Cu^{+}(NO)_n$ ($n = 1, 2$) complexes.

The doublets at 1708–1809 and 1743–1885 cm^{-1} initially increase (Fig. 5a, curves 2 and 3) and then decrease (Fig. 5b, curves 4–15). The peak at 1775 cm^{-1} increases slightly with temperature and does not disappear even at RT (Fig. 5b). The increase with temperature of the absorption in the 1915–1880 cm^{-1} range (Fig. 5a) is indicative of the formation of stable $Cu^{2+}(NO)$ complexes as a consequence of redox reactions occurring on the surface. Simultaneously (see insets), bands typical of adsorbed N_2 (about 2350 cm^{-1}) and of adsorbed N_2O (about 2250 cm^{-1}) appears (Fig. 5a) (vide infra). The intensities of the peaks associated with the weakly adsorbed species decline as the temperature increases and tends to disappear at RT.

To facilitate a detailed assignment of the bands illustrated in Fig. 5a, an identical temperature-dependent experiment has been ad hoc repeated on Cu_2O/SiO_2. The spectra resulting from this experiment are reported in Fig. 6a and b.

At the lowest temperatures (Fig. 6a), two bands are observed at 1775 and 1881 cm^{-1} due to adsorbed

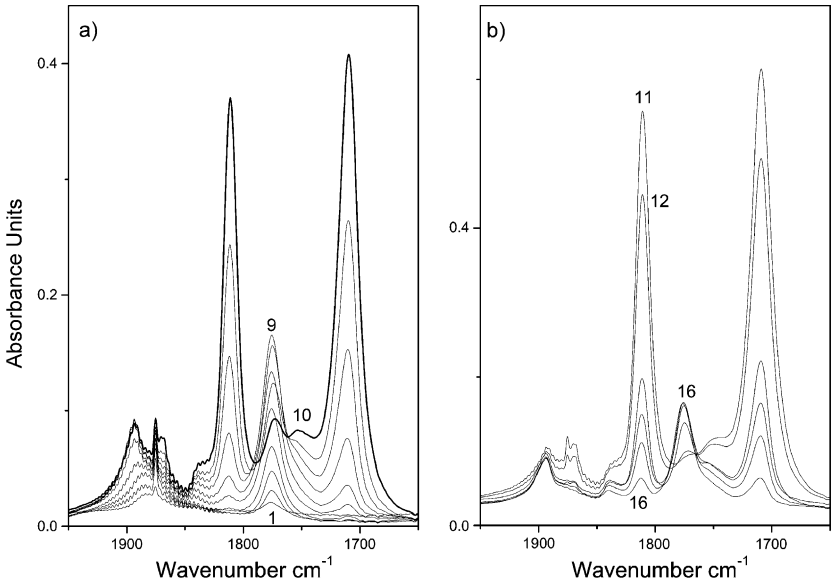

Fig. 6. IR spectra of NO dosed on Cu_2O/SiO_2 sample as a function of the temperature increase from liquid nitrogen temperature to RT. (a) First stage; (b) final stages. Spectrum 1: $P_{NO} \cong 7 \times 10^{-2}$ Torr ($T \cong 77$ K); spectrum 3: $P_{NO} \cong 1$ Torr ($T \cong 150$ K); spectra 4–12: $P_{NO} \cong 1$ Torr ($150 \leq T \leq 273$ K); spectra 12–16: outgassing at RT.

NO. The latter is ascribed to $Cu^{2+}\cdots NO$ adducts formed on a small fraction of non-reduced cupric cations (vide infra), while the former is assigned to the $Cu^{+}\cdots NO$ complex formed on mono-coordinated Cu^{+} sites of the unpolar $Cu_2O(1\,1\,1)$ face. Upon increasing temperature and pressure, the 1775 cm^{-1} band increases reaching a maximum and then declines. Simultaneously, a doublet shows up at 1709 and 1811 cm^{-1}. The components of the doublet are ascribed to the $Cu^{+}\cdots(NO)_2$ ($\bar{\nu}_l(NO)_2 = 1709\,cm^{-1}$ and $\bar{\nu}_h(NO)_2 = 1811\,cm^{-1}$) formed following the reaction $Cu^{+}\cdots NO + NO \rightarrow Cu^{+}\cdots(NO)_2$. These assignments are confirmed by the spectra reported in part (b) of Fig. 6 where a further temperature increase (at constant P_{NO}) makes the mono-nitrosyl more stable and inverse $Cu^{+}\cdots(NO)_2 \rightarrow Cu^{+}\cdots NO$ reaction takes place.

As was the case for CO, a brief overview on the literature concerning the IR spectroscopy of NO on Cu-zeolites, see e.g. Refs. [32,33,36,39,43,44,47,50, 57–59], can guide the interpretation of the spectra reported in Fig. 5a and b. For this reason, Fig. 7 summarizes the IR spectra obtained by dosing NO on Cu^{+}-ZSM-5, Cu^{+}-β, Cu^{+}-mordenite and Cu^{+}-Y

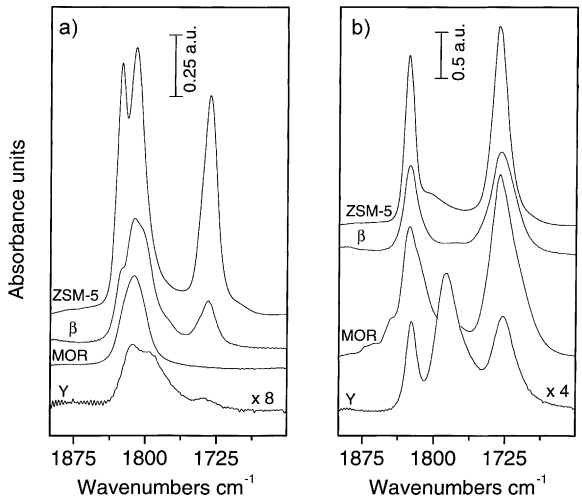

Fig. 7. IR spectra of NO dosed, at about 100 K on, from top to bottom; Cu^{+}-ZSM-5, Cu^{+}-β, Cu^{+}-mordenite and Cu^{+}-Y zeolites. Parts (a) and (b) show low and high equilibrium pressures, respectively.

zeolites: low and high equilibrium pressures (parts (a) and (b), respectively).

The IR spectroscopy of nitrosyl complexes formed at low temperature on Cu^+ sites in zeolites shows a poly-addition similar to that observed for carbonyls, however, $Cu^+\cdots(NO)_3$ complexes have not been observed. At low equilibrium pressure, the formation of $Cu^+\cdots NO$ adducts gives a single N–O band in the 1811–1814 cm^{-1} range (see $\bar{\nu}$(NO) in Table 1), with the only exception of Cu^+-Y, where NO adsorbed on the more shielded II* position results in a second component at $\bar{\nu}(NO) = 1788\,cm^{-1}$ [37]. This result is analogous to what was obtained with CO.

The increase of NO equilibrium pressure causes the splitting of the mono-nitrosyl band into the asymmetric and symmetric stretching modes of the $Cu^+\cdots(NO)_2$ complex ($\bar{\nu}_l(NO)_2$ and $\bar{\nu}_h(NO)_2$ in the 1728–1734 and 1824–1827 cm^{-1} range, respectively, see Table 3). For ZSM-5 and β, even at the lowest NO equilibrium pressure, we observe the presence of the two $Cu^+\cdots(NO)_2$ bands superimposed to that of the mono-nitrosyl. The increase of the NO equilibrium pressure yields to the total $Cu^+\cdots NO \rightarrow Cu^+\cdots(NO)_2$ transformation (Fig. 7b). This does not hold for MOR and Y, where the transformation is only partial.

At this point, the interpretation of the IR spectra obtained by dosing NO on Na-Cu-ETS-10(B) sample (Fig. 5a) is straightforward: the five components observed in the low-temperature spectra are in fact two doublets due to $Cu^+\cdots(NO)_2$ adducts formed on Cu_2O ($\bar{\nu}_l(NO)_2 = 1708\,cm^{-1}$ and $\bar{\nu}_h(NO)_2 = 1810\,cm^{-1}$, strong) and on Cu^+ counterions ($\nu_l(NO)_2 = 1740\,cm^{-1}$ and $\nu_h(NO)_2 = 1830\,cm^{-1}$, weak) and two unresolved bands in the 1790–1770 cm^{-1} region due to the corresponding $Cu^+\cdots NO$ complexes. As expected, both doublets increase during the first stages of the experiment (Fig. 5a) and then decrease at higher temperatures (Fig. 5b), where the absorption due to the two mono-nitrosyl complexes dominates. The symmetric and asymmetric stretching frequencies of di-nitrosyl complexes formed on Cu_2O nano-crystals is very close to those observed on Cu_2O/Si_2O sample, while the corresponding doublet ascribed to adducts formed on Cu^+ counterions lies at frequencies about 10 cm^{-1} higher with respect to those measured for the same adducts in the other Cu^+-zeolites (see Table 3). The exact location of mono-nitrosyl complexes is not feasible, due to the strong overlap between the bands due to the complexes formed on the two cuprous sites. As a consequence, the corresponding wavenumbers reported in Table 3 are only indicative. However, the fact that the broad band in the 1790–1770 cm^{-1} region is due to the superimposition of more than one component is supported by the evidence that the absorption is broad and its maximum (Fig. 5b) shifts from 1778 to 1787 cm^{-1} by increasing the temperature. The shift can be ascribed to a variation of the

Table 3
N–O, $\bar{\nu}_a(NO)_m$ ($m = 1, 2$), stretching frequencies of nitrosylic adducts in Cu^+-zeolites and in Cu_2O (pure and supported)[a]

Sample	$\bar{\nu}$(NO) (cm^{-1})	$\bar{\nu}_l(NO)_2$ (cm^{-1})	$\bar{\nu}_h(NO)_2$ (cm^{-1})	Reference
Cu^+-ZSM-5	1812	1734	1827	[36]
Cu^+-β	1811	1730	1826	[39]
Cu^+-mordenite	1812	1731	1826	[39]
Cu^+-Y Site II	1814	1728	1824	[37]
Cu^+-Y Site II*	1788	Not observed	Not observed	[37]
Na-Cu-ETS-10(B) isolated Cu^+ site	≅1787	1740	1830	This work
Na-Cu-ETS-10(B) Cu_2O site	≅1778	1708	1810	This work
Cu_2O/SiO_2	1775	1709	1811	This work
Cu^{2+}-ZSM-5	1890	Not observed	Not observed	[36]
Na-Cu^{2+}-ETS-10(B)	1880	Not observed	Not observed	This work
Cu^{2+} on Cu_2O/SiO_2	1894	Not observed	Not observed	This work
Na-ETS-10	1898	Not observed	Not observed	[21]

[a] Label "a" (a: l, h) refers to low and high frequency components of the di-nitrosylic adducts. For ZSM-5, Na-Cu-ETS-10(B) and Cu_2O/SiO_2 samples, also the IR frequency of the $Cu^{2+}\cdots(NO)$ adduct formed upon oxidation of Cu^+ by NO have been reported. For comparison also the most intense IR component obtained upon dosing NO on the Na-ETS-10 sample, before cation exchange with $Cu(NO_3)_2$, has also been reported.

relative ratio between mono-nitrosyl adducts formed on the two Cu^+ sites. It is now worth noticing that the 1778 cm^{-1} frequency is very close (3 cm^{-1}) to that found for the $Cu^+ \cdots NO$ complexes formed on Cu_2O/Si_2O sample (see Fig. 6 and Table 3). As a consequence, the assignment of the 1778 cm^{-1} component to mono-nitrosyl complexes formed on Cu_2O nano-particles is rather safe. The same does not hold for the frequency of the $Cu^+ \cdots NO$ complexes formed on the less abundant Cu^+ counterions.

Once the discussion and the assignments of the components due to NO adsorbed on cuprous sites has been made (1850–1650 cm^{-1} region in Figs. 5 and 6), we can discuss the 1950–1850 cm^{-1} region, i.e. the region where $Cu^{2+} \cdots NO$ complexes are expected [32,36,57]. This band is virtually absent in the spectra taken at lowest temperature on Na-Cu-ETS-10(B) sample (Fig. 5a) and in Cu_2O/Si_2O sample (Fig. 6a). Upon increasing the temperature, in both cases, a continuous increase of this band is observed; this indicates that NO begins to oxidize Cu^+ cations to Cu^{2+}. In other words, both samples become active catalyst in the decomposition of NO. This conclusion is based on the analogy with the results obtained on Cu^+-ZSM-5 [36]. This statement is supported by the evolution of the IR bands in the 2380–2190 cm^{-1} region (see inset in Fig. 5a and b), where some products of the NO decomposition reaction (N_2 and N_2O) are expected. The most intense band lies in the 2260–2230 cm^{-1} range and is ascribed to the presence of weakly bonded N_2O species [36]. In the same inset, a composite absorption at 2370–2345 cm^{-1} is also evident; following Ref. [36], we attribute the latter band to N_2 molecules adsorbed on Cu^{2+} sites. The complexity of both bands can be ascribed to the heterogeneity of Cu sites in the Na-Cu-ETS-10(B) sample. As far as the 2370–2345 cm^{-1} band is concerned, a contribution of NO^+ species cannot be excluded [60]. These species could be formed in a side process through disproportionation of liquid-like NO into $NO^+ + (N_2O_2)^-$ or into $NO^+ + N_2O + NO_2^-$ ionic species [61]. The absence of the band in the 2300–2275 cm^{-1} region upon direct adsorption of N_2 rules out any assignment based on di-nitrogen molecules adsorbed on Cu^+ sites. Of course, the formation of N_2 indicates that the NO decomposition into N_2 and O_2 is already initiating following the plausible scheme:

$$2NO \rightarrow N_2 + O_2$$

The spectroscopy of NO dosed on Na-Cu-ETS-10(A) sample does not show new relevant bands, consequently these spectra are not discussed in detail. We only notice that the bands due to nitrosyl complexes on Cu_2O have smaller (relative) intensity.

4. Conclusion

A complete IR study of N_2, CO and NO adsorbed on a Cu-exchanged ETS-10 activated at 673 K under dynamic vacuum is reported. In spite of the complexity of the IR spectra, an exhaustive assignment of the observed components has been made on the basis of an accurate comparison with similar experiments carried on several Cu^+-zeolites and Cu_2O particles dispersed on silica and on MCM-41. Two different families of cuprous sites are evidenced: (i) Cu^+ sites of Cu_2O nano-crystals formed during sample activation; (ii) Cu^+ counterions, balancing the negative charge of the framework. The size of the Cu_2O nano-crystals entrapped in the channels and cavities must be very small, as evidenced by: (i) the blue shift of the adsorption edge, with respect to bulk Cu_2O, observed by UV–Vis; (ii) the absence of CO–CO interactions (which are on the contrary present on extended facelets and terraces of well-shaped microcrystals). For these reasons, the hypothesis that part of the Cu_2O nano-particles are trapped inside the ETS-10 channels is reasonable. The cuprous sites are active in the decomposition of NO, as demonstrated by a temperature-dependent IR study.

Acknowledgements

This project has been supported by MURST (Cofin 98, Area 03). We are indebted to J. Rocha and M.W. Anderson for having supplied a copy of manuscript [7] prior publication.

Note added in proof

After the submission of this work some important papers have appeared in the literature [62–64]. Ref.

[62] reports a combined XPS and XANES study on the thermal $Cu^{2+} \rightarrow Cu^{+}$ reduction and should be quoted together with Refs. [42,48–51]. It also reports a combined IR and microcalorimetric study on the adsorption of CO on Cu-ZSM-5 zeolite. Ref. [63] is a review article on metal carbonyls where the reader can be found the C–O stretching frequencies of different $Cu^{+}\ldots(CO)_n$ ($n = 1,2,3,4$) complexes, to be compared with those reported here in Table 2. Finally, Ref. [64] is a review article on the surface characterisation of oxides and halides. In that work several N–N, C–O and N–O stretching frequencies have been collected, to be compared with those reported here in Tables 1, 2 and 3.

References

[1] S.M. Kuznicki, US Patent 4,853,202 (1989).
[2] D.M. Champman, A.L. Roe, Zeolites 10 (1990) 730.
[3] M.W. Anderson, O. Terasaki, T. Ohsuna, A. Phillippou, S.P. MacKay, A. Ferreira, J. Rocha, S. Lidin, Nature 367 (1994) 347.
[4] M.W. Anderson, O. Terasaki, T. Ohsuna, P.J.O. Malley, A. Phylippou, S.P. MacKay, A. Ferreira, J. Rocha, S. Lidin, Phil. Mag. B 71 (1995) 813.
[5] T. Ohsuna, O. Terasaki, D. Watanabe, M.W. Anderson, S. Lidin, Stud. Surf. Sci. Catal. 84 (1994) 413.
[6] X.Q. Wang, A.J. Jacobson, Chem. Commun. (1994) 973.
[7] J. Rocha, M.W. Anderson, Eur. J. Inorg. Chem. 5 (2000) 801.
[8] G. Sankar, R.G. Bell, J.M. Thomas, M.W. Anderson, P.A. Wright, J. Rocha, J. Phys. Chem. 100 (1996) 449.
[9] E. Borello, C. Lamberti, S. Bordiga, A. Zecchina, C. Otero Areán, Appl. Phys. Lett. 71 (1997) 2319.
[10] C. Lamberti, Micropor. Mesopor. Mater. 30 (1999) 155.
[11] S. Bordiga, G. Turnes Palomino, A. Zecchina, G. Ranghino, E. Giamello, C. Lamberti, J. Chem. Phys. 112 (2000) 3859.
[12] T. Blasco, M.A. Cambor, A. Corma, J. Perez-Pariente, J. Am. Chem. Soc. 115 (1993) 11806.
[13] M. Taramasso, G. Perego, B. Notari, US Patent 4,410,501 (1983).
[14] B. Notari, Adv. Catal. 41 (1996) 253.
[15] S. Bordiga, S. Coluccia, C. Lamberti, L. Marchese, A. Zecchina, F. Boscherini, F. Buffa, F. Genoni, G. Leofanti, G. Petrini, G. Vlaic, J. Phys. Chem. 98 (1994) 4125.
[16] V. Bolis, S. Bordiga, C. Lamberti, A. Zecchina, G. Petrini, F. Rivetti, G. Spanò, Langmuir 15 (1999) 5753.
[17] M.E. Grillo, J. Carrazza, J. Phys. Chem. 100 (1996) 12261.
[18] M.W. Anderson, J.R. Agger, D.P. Luigi, A.K. Baggaley, J. Rocha, Phys. Chem. Chem. Phys. 1 (1999) 2287.
[19] G. Ganapathy, T.K. Das, R. Vetrivel, S.S. Ray, T. Sen, S. Sivasanker, L. Delevoye, C. Fernandez, J.P. Amoureux, J. Am. Chem. Soc. 120 (1998) 4752.
[20] M.A. Fox, K.E. Doan, M.T. Dulay, Res. Chem. Intermediat. 20 (1994) 711.
[21] A. Zecchina, C. Otero Areán, G. Turnes Palomino, C. Lamberti, G. Spoto, D. Scarano, S. Bordiga, F. Geobaldo, Phys. Chem. Chem. Phys. 1 (1999) 1649.
[22] A. Philippou, M. Naderi, N. Pervaiz, J. Rocha, M.W. Anderson, J. Catal. 178 (1998) 174.
[23] T.K. Das, A.J. Chandwadkar, S. Sivasanker, Stud. Surf. Sci. Catal. Lett. 113 (1998) 455.
[24] S.B. Waughmode, T.K. Das, S. Sivasanker, Catalysis 185 (1999) 265.
[25] A. Philippou, J. Rocha, M.W. Anderson, Catal. Lett. 57 (1999) 151.
[26] S.M. Kuznicki, K.A. Thrush, US Patent 4,994,191 (1991).
[27] C. Otero Areán, G. Turnes Palomino, A. Zecchina, S. Bordiga, F.X. Llabrés i Xamena, C. Pazé, Catal. Lett. 66 (2000) 231.
[28] C.L. Bianchi, R. Carli, S. Merlotti, V. Ragaini, Catal. Lett. 41 (1996) 79.
[29] C.L. Bianchi, V. Ragaini, J. Catal. 168 (1997) 70.
[30] C.L. Bianchi, S. Vitali, V. Ragaini, Stud. Surf. Sci. Catal. 119 (1998) 167.
[31] C.L. Bianchi, S. Ardizzone, V. Ragaini, Stud. Surf. Sci. Catal. 119 (1998) 173.
[32] M. Shelef, Chem. Rev. 95 (1995) 209.
[33] G. Centi, S. Perathoner, Catal. Today 29 (1996) 117.
[34] M. Iwamoto, H. Yahiro, S. Sundo, Y. Yu-u, N. Mizuno, Appl. Catal. 69 (1991) L15.
[35] V.I. Parvulescu, P. Grange, B. Delmon, Catal. Today 46 (1998) 233.
[36] C. Lamberti, S. Bordiga, M. Salvalaggio, G. Spoto, A. Zecchina, F. Geobaldo, G. Vlaic, M. Bellatreccia, J. Phys. Chem. B 101 (1997) 344.
[37] G. Turnes Palomino, S. Bordiga, A. Zecchina, G.L. Marra, C. Lamberti, J. Phys. Chem. B 104 (2000) 8641.
[38] C. Lamberti, S. Bordiga, A. Zecchina, M. Salvalaggio, F. Geobaldo, C. Otero Areán, J. Chem. Soc., Faraday Trans. 94 (1998) 1519.
[39] G. Turnes Palomino, E. Giamello, P. Fisicaro, S. Bordiga, C. Lamberti, A. Zecchina, Stud. Surf. Sci. Catal. 130 (2000) 2915.
[40] A. Zecchina, D. Scarano, G. Spoto, S. Bordiga, C. Lamberti, G. Bellussi, Stud. Surf. Sci. Catal. 117 (1998) 434.
[41] D. Scarano, S. Bordiga, C. Lamberti, G. Spoto, G. Ricchiardi, A. Zecchina, C. Otero Areán, Surf. Sci. 411 (1998) 272.
[42] G. Turnes Palomino, P. Fisicaro, S. Bordiga, A. Zecchina, E. Giamello, C. Lamberti, J. Phys. Chem. B 104 (2000) 4064.
[43] G. Spoto, S. Bordiga, D. Scarano, A. Zecchina, Catal. Lett. 13 (1992) 39.
[44] G. Spoto, A. Zecchina, S. Bordiga, G. Ricchiardi, G. Martra, G. Leofanti, G. Petrini, Appl. Catal. B 3 (1994) 151.
[45] A. Zecchina, S. Bordiga, M. Salvalaggio, G. Spoto, D. Scarano, C. Lamberti, J. Catal. 173 (1998) 540.
[46] A. Zecchina, S. Bordiga, G. Turnes Palomino, D. Scarano, C. Lamberti, M. Salvalaggio, J. Phys. Chem. B 103 (1999) 3833.
[47] J. Valyon, W.K. Hall, J. Phys. Chem. 97 (1993) 1204.
[48] W. Grünert, N.W. Hayes, R.W. Joyner, E.S. Shpiro, M. Rafiq, H. Siddiqui, G.N. Baeva, J. Phys. Chem. 98 (1994) 10832.
[49] J. Valyon, W.K. Hall, J. Phys. Chem. 97 (1993) 7054.

[50] H.J. Jong, W.K. Hall, J.L. d'Itri, J. Phys. Chem. 100 (1996) 9416.
[51] C. Dossi, A. Fusi, G. Moretti, S. Recchia, R. Psaro, Appl. Catal. A 188 (1999) 107.
[52] F. Geobaldo, C. Lamberti, G. Ricchiardi, S. Bordiga, A. Zecchina, G. Turnes Palomino, C. Otero Areán, J. Phys. Chem. 99 (1995) 11167.
[53] A. Zecchina, C. Otero Areán, Chem. Soc. Rev. 25 (1996) 187.
[54] Y. Kuroda, Y. Yoshikawa, S. Konno, H. Hamano, H. Maeda, R. Kumashiro, M. Nagao, J. Phys. Chem. 99 (1995) 10621.
[55] C. Lamberti, G. Turnes Palomino, S. Bordiga, G. Berlier, F. D'Acapito, A. Zecchina, Angew. Chem. Int. Ed. Engl. 39 (2000) 2138.
[56] S. Bordiga, D. Scarano, G. Spoto, A. Zecchina, C. Lamberti, C. Otero Areán, Vib. Spectrosc. 5 (1993) 69.
[57] E. Giamello, D. Murphy, G. Magnacca, C. Morterra, Y. Shioya, T. Nomura, M. Anpo, J. Catal. 136 (1992) 510.
[58] C. Henriques, M.F. Ribeiro, C. Abreu, D.M. Murphy, F. Poignant, J. Saussey, J.C. Lavalley, Appl. Catal. B 16 (1998) 79.
[59] M. Ziólek, I. Sobczak, I. Nowak, M. Daturi, J.C. Lavalley, Topics Catal. 11/12 (2000) 343.
[60] J. Laane, J.R. Ohlsen, Prog. Inorg. Chem. 27 (1980) 645.
[61] P.H. Kasai, R.J. Bishop, J. Am. Chem. Soc. 94 (1972) 5560.
[62] V. Bolis, S. Maggiorin, L. Meda, F. D'Acapito, G. Turnes Palomino, S. Bordiga, C. Lamberti, J. Chem. Phys. 113 (2000) 9248.
[63] A.J. Lupinetti, S.H. Strauss, G. Frenking, Prog. Inorg. Chem. 49 (2001) 1.
[64] A. Zecchina, D. Scarano, S. Bordiga, G. Spoto, C. Lamberti, Adv. Catal. 46 (2001) 265.